Fine structures in the intensity dependence of excitation and ionization probabilities of hydrogen atoms in intense 800-nm laser pulses

Qianguang Li,[1] Xiao-Min Tong,[2] Toru Morishita,[3] Hui Wei,[4] and C. D. Lin[4]

[1]*School of Physics and Electronic-information Engineering, Hubei Engineering University, Xiaogan 432000, China*
[2]*Faculty of Pure and Applied Sciences, and Center for Computational Science, University of Tsukuba, 1-1-1 Tennodai, Tsukuba, Ibaraki 305-8577, Japan*
[3]*Department of Engineering Science, The University of Electro-Communications, 1-5-1 Chofu-ga-oka, Chofu-shi, Tokyo 182-8585, Japan*
[4]*J. R. Macdonald Laboratory, Physics Department, Kansas State University, Manhattan, Kansas 66506-2604, USA*

We studied the elementary processes of excitation and ionization of atomic hydrogen in an intense 800-nm pulse with intensity in the 1.0 to 2.5×10^{14} W/cm^2 range. By analyzing excitation as a continuation of above-threshold ionization (ATI) into the below-threshold negative energy region, we show that modulation of excitation probability and the well-known shift of low-energy ATI peaks vs laser intensity share the same origin. Modulation of excitation probability is a general strong field phenomenon and is shown to be a consequence of channel closing in multiphoton ionization processes. Furthermore, the excited states populated in general have large orbital angular momentum and they are stable against ionization by the intense 800-nm laser—they are the underlying reason for population trapping of atoms and molecules in intense laser fields.

PACS number(s): 32.80.Rm

I. INTRODUCTION

Photoexcitation and photoionization processes of an atomic hydrogen over the whole electromagnetic spectrum are the standard topics in undergraduate modern physics and quantum mechanics textbooks. Before the invention of intense lasers, the interaction of light with matter was often treated by perturbation theory. Since the 1960s, with the invention of intense laser pulses, two-photon and multiphoton absorption processes began to draw great interest. In the last two to three decades, with Ti:sapphire lasers (wavelength around 800 nm), short pulses with duration from a few to tens of femtoseconds became widely available. These pulses can be focused to reach very high intensity such that strong field physics of atoms and molecules have emerged as a new discipline. Processes such as high-order harmonic generation, above-threshold ionization (ATI), multiple ionization, and other phenomena have been widely investigated. Lately, with the advent of laser technology, strong field physics has been extended to midinfrared wavelength lasers (up to a few microns). Similarly, advance of accelerator technology has opened up nonlinear physics—for free-electron lasers with wavelength from the extreme ultraviolet (EUV) to x rays. These progresses make it possible to study nonlinear physics over a broadband of electromagnetic spectrum.

From the theoretical viewpoint, the nonlinear interaction of a hydrogen atom with an intense field of light of different wavelength is considered a basic problem that can be rigorously solved numerically. Within the nonrelativistic approximation, for a given light pulse, all the physical processes are included in the "exact" solution of the time-dependent Schrödinger equation (TDSE). Such results are considered as good or even "better" than experimental data. These numerical data can be used to test simpler theoretical models to draw general conclusions that may be applicable at least qualitatively to more complex targets.

In spite of this minimal goal, an "exact" solution of TDSE in intense laser field has to be taken with caution. From the

numerical standpoint, how does one know that the calculation indeed is converged? The dimension of the Hilbert space of a hydrogen atom is infinite. Besides the dominant processes, there are processes where transition probabilities are much smaller. More precisely, the hydrogen atom can be ionized or excited after the pulse is over. The atom can be left at various excited states, from the low-lying levels to very high Rydberg states, or ionized with the electron emerging at different energies and angles. Convergence can be tested for a selected subset of data of interest. For example, total excitation and total ionization probabilities may be "converged," but it does not guarantee that excitations to individual states or ionization to various electron energy or momentum are converged. On the other hand, there are possible features that are not specific to atomic hydrogen only. Here our goal is to draw from the numerical "experimental" data some general conclusions that are common to other complex targets.

In strong field experiments, a laser pulse is sharply focused into a gas cell or a gas jet. The experimental data are obtained by integrating over the distributed intensities within the focal volume. Precise characterization of temporal and spatial distributions of a laser beam in general is not possible. Thus many finer features predicted from the accurate TDSE calculation may be averaged out after volume integration. In other cases, they are normally not measured by experimentalists, for example, excitations to individual excited states. On the other hand, some features that do not change rapidly with laser intensity may survive the volume integration. Examples of such features are abundant. For example, ATI electrons [1], Freeman resonances [2], "fanlike" angular distributions of low-energy photoelectrons [3–5], "holography" in the photoelectron momentum distributions [6–8], and the conspicuous low-energy structures (LES) of photoelectrons by midinfrared pulses [9–11]. In addition, there are fine features observed only in very carefully detailed measurements. For example, both multiphoton ionization and tunneling ionization model predict that total ionization probability should grow monotonically with laser intensity, but measurement of ion yields with small

steps of intensity increment revealed minute yet reproducible modulation from a smooth curve [12,13]. Such irregularity was later interpreted as due to "population trapping" where electrons are not ionized, but trapped in the excited states. To interpret population trapping an elaborate interference stabilization (IS) [14] model employing second-order Λ-type Raman transitions was proposed. While this model has been used to interpret many experiments qualitatively, we note that no actual calculations have ever been actually carried out to confirm the IS model.

The existence of low or high Rydberg states in an intense laser field was often viewed as unlikely, especially at high intensity where the atom in the ground state is already severely depleted. On the other hand, the presence of excited states of an atom in an intense laser field has been reported experimentally since the 1990s [15–17]. In our opinion, however, how these excited states are populated and how they remain stable in the intense laser field still have not been fully investigated yet. Thus, a careful examination based on accurate numerical TDSE results will be illustrative. Since excitation probabilities for higher excited states are small, it is important to perform TDSE calculations that are converged. In this article we obtained results from two independent well-tested TDSE codes. They are then analyzed by treating excitation and ionization on equal footing. We mention that a similar method of analyzing laser induced excited states has been employed by Morishita and Lin [18] for the strong field ionization of Li by an 800-nm laser. Since the ionization energy of Li is only 5.39 eV, at an intensity of a few times of 10^{12} W/cm^2 the ground state of Li is already fully depleted. The interplay between excitation and ionization in Li is thus different from the hydrogen atom studied here. However, it has shown in Ref. [18] that a few percent of Li would remain neutral, with the Li in highly excited states. In other words, in general atoms and molecules are stable against ionization by intense laser fields if they are in highly excited states.

The goal of this work is twofold. First, we carried out TDSE calculations to study electron spectra and the integrated total ionization yields vs laser intensity. The origin of "small steps" in the ion yields vs laser intensity is identified: They are associated with intensities when "channel closing" occurs, i.e., at an intensity where absorption of one more photon is needed to ionize the atom due to the increase of the ponderomotive energy. Second, we study excitation probabilities for low-lying and Rydberg states. We will show that small steps in ionization always occur when the total excitation probabilities are at the local maximum. The increase in excitation probability above channel closing can be understood as resulting from the shift of the first ATI peak below the ionization threshold.

The rest of this paper is organized as follows. In Sec. II a short summary of the methods used for solving the TDSE equation will be described. In Sec. III detailed comparison of data from the two calculations will be analyzed, with emphasis on photoelectrons near the ionization threshold and the excited states. The last section summaries the results and the mechanism of "population trapping." Atomic units are used in the article unless indicated otherwise.

II. THEORETICAL METHODS

We solved the time-dependent Schrödinger equation (TDSE) for atomic hydrogen in an intense laser field to calculate photoelectron spectra and the population of excited states with the hydrogen atom initially in the ground state. Two different computation methods are used. In the first, the TDSE is solved in the time-integral form [19]. The real space is divided into an inner region $R < R_c$ and an outer region $R_c < R < R_{max}$. The time-dependent wave function is propagated within the box $R < R_{max}$ using the second-order split operator method in the energy representation [20]. In the outer region, the continuum states are expanded into continuum Coulomb wave functions and then further propagated analytically as Volkov momentum states [19]. The bound states and electron momentum distributions are obtained by analyzing the time-dependent wave function after the laser pulse is over. The box size chosen is $R_{max} = 800$ a.u., $R_c = 500$ a.u.. For each IR cycle 2000 time steps were used. The radial grid points is 2000 and 50 partial waves are used in the expansion. The results from this method are obtained using the velocity gauge for describing laser-atom interaction [21]. The maximum electron energy in the calculation is 5 a.u. and the highest Rydberg states that can be described accurately are $n = 25$, but we include all negative energy states in the total excitation probability calculation. To check convergence, we enlarge R_{max}, the number of grid points in space and in time steps, and the number of partial waves.

In the second method, length gauge is used for describing laser-atom interaction. The electronic wave function is also expanded in spherical coordinates where the radial functions are further expanded in terms of direct products of discrete variable representation (DVR) functions [3,22]. Using the split operator method the time propagation is integrated in the space of the energy eigenstates of atomic hydrogen. With the length gauge, the time steps can be made larger, but the number of angular momentum states has to increase substantially. In our typical calculation, for 10 fs pulse, we chose $R_{max} = 1500$, number of r grids $= 3000$, maximum angular momentum $= 240$, and number of time grids $= 2000$. For 20 fs pulses, the respective numbers are 3000, 4800, 400, and 4000. To check convergence, we also vary the box size, the number of grid points in space and time of integration, and the maximum orbital angular momentum. The total ionization probability is checked to be accurate to better than 1%. For the smaller excitation probability and electron energy distribution, we estimated that the accuracy is within 5% to 10%. (Figure 10 shows results from the two gauges and their relative convergence.)

A linearly polarized laser field is used in the calculation. Its electric field is taken the form [22]

$$\mathbf{F}(t) = F_0 \hat{z} a(t) \cos(\omega t + \varphi), \tag{1}$$

where ω is the carrier frequency and φ is the carrier-envelope phase with the envelope function $a(t)$ chosen to be

$$a(t) = \cos^2\left(\frac{\pi t}{\tau}\right) \tag{2}$$

for the time interval $(-\tau/2, \tau/2)$ and zero elsewhere. The pulse duration, defined as the full width at half maximum (FWHM),
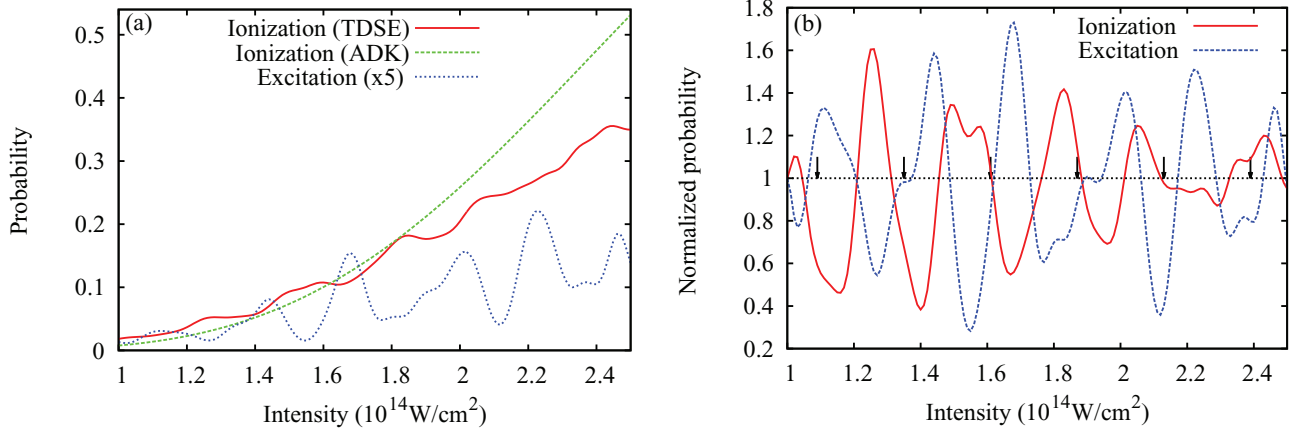
FIG. 1. (Color online) Intensity dependence of total excitation and ionization probabilities of atomic hydrogen by a 10 fs, 800-nm laser pulse. (a) Results from TDSE calculations and comparison with the ADK tunneling ionization model. The excitation probability has been multiplied by 5 for easier visualization. (b) Renormalized excitation and ionization probabilities (expressed as ratios with respect to a smooth background) to display nonmonotonic oscillatory features vs laser intensity (see text). Arrows indicate positions of channel closing thresholds, with the first one for absorption of 13 photons. The peaks of excitation and ionization are out of phase, at least below intensity of 2×10^{14} W/cm^2.

is given by $\Gamma = \tau/2.75$. The carrier envelope phase is always set at zero in the calculation.

III. RESULTS AND DISCUSSION

A. Oscillation of total ionization and excitation probabilities vs laser intensity

Figure 1(a) presents the calculated total ionization and excitation probability for 10 fs pulses with intensities from 1.0 to $2.5I_0$, where $I_0 = 10^{14}$ W/cm^2. Within this range, the ionization probability rises from about 2% to 35% when the laser intensity only increases 2.5 times. With calculations carried out with a step size of $0.01I_0$, we note that ionization probability does not increase monotonically, but instead shows local weak steps where ionization stays relative flat before rapid rise again. The Keldysh parameters for the studied intensity range is from 1.07 to 0.68. We also compare the TDSE results with those obtained according to the ADK tunneling theory [23]. For comparison, total excitation probabilities (multiplied five times) are also shown in Fig. 1(a). They display strong modulations that are out of phase in relation to the oscillation in the ionization probability.

To demonstrate the out-of-phase oscillation between excitation and ionization probabilities, we first obtain a smoothed curve for each, respectively, then the ratios of excitation and ionization probabilities with respect to the smoothed probabilities are displayed. More precisely, in Fig. 1(b), for excitation we plot the ratio $P(I)/P_{sm}$, for ionization we plot $5 * [P(I)/P_{sm} - 1] + 1$, where $P(I)$ is the respective excitation or ionization probability, and P_{sm} is the respective smoothed probability. The out-of-phase oscillations between the two probabilities can now be clearly seen. In the figure, channel closing intensity I_c for absorption of n photons are indicated. Here channel closing occurs for $n\hbar\omega = I_p + U_p$, where $\hbar\omega = 1.55$ eV is the photon energy, $I_p = 13.6$ eV is the ionization energy of hydrogen, and $U_p = I/(4\omega^2)$ is the ponderomotive energy of the laser field of intensity I. The

lowest n in the figure is 13, the next one is 14, and so on. Below $2.0I_0$, between two channel-closing thresholds, ionization and excitation probabilities each goes through a maximum and a minimum. These structures are easily understood in terms of a multiphoton ionization picture.

The features presented above have been investigated previously by Popov *et al.* [24] for atomic hydrogen. Their calculations were carried out using TDSE also, but by representing a wave function on the grid points in the radial coordinate. A regularized Coulomb potential $V(r) = -1/\sqrt{r^2 + \alpha^2}$ is employed to represent the electron-nucleus interaction. In spite of such an approximation, the oscillation in the excitation probabilities and the small steps in the ion yields vs laser intensity have been observed in their calculations also. Similar calculations have been carried out for the Xe atom to explain the experimentally observed nonmonotonic dependence of ion yields vs laser intensity, as reported by Azarm *et al.* [25]. The electron and Xe ion core interaction is again represented by a regularized Coulomb potential with the parameter α chosen such that the ground state energy of Xe is correctly reproduced.

B. Low-energy photoelectron energy distributions

In Fig. 2, photoelectron energy distributions below 8 eV are displayed vs laser peak intensities. As the intensity increases, the electron distribution shifts toward lower energies, in accordance with the increase of ponderomotive energy which depends linearly with the intensity. Close to the channel closing threshold (marked by arrows on the horizontal axis), the photoelectron has maximum yield near the ionization threshold. With intensity increases beyond the channel closing threshold, these "above-threshold ionization" (ATI) electrons would "dive" into the below-threshold region. These electrons would appear as excited states. Thus it is instructive to consider excitation and ionization on the same footing, by redefining excitation probability P_n for each state in terms of excitation probability density $dP_n/dE = P_n(dn/dE) = P_n n^3$, where
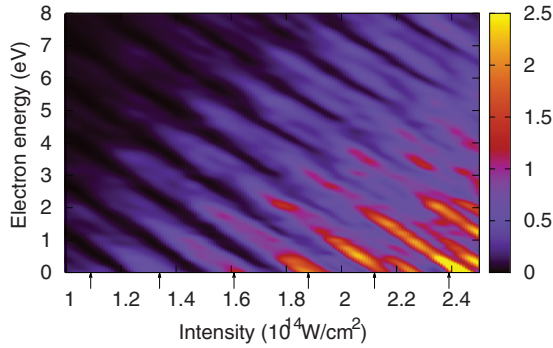
FIG. 2. (Color online) Electron spectra vs peak laser intensity for 10 fs pulses. Arrows along the horizontal axis indicate the positions of channel closing thresholds. At lower intensities, for channel closing intensity the first ATI peak is located at the ionization threshold. At higher intensities additional features related to Freeman resonances appear.

$E = -(1/2n^2)$ is the energy of the excited state with principal quantum number n.

In Fig. 3 we show how the electron spectra evolve from -0.04 (close to $n = 4$) to 0.12 a.u. for laser intensities between two channel closing thresholds at $1.61I_0$ and $1.88I_0$. At each intensity, above the threshold, individual ATI peaks are clearly visible. The first ATI peak moves toward lower energy as the laser intensity is increased, and then continues smoothly below the threshold. From $1.61I_0$ to $1.70I_0$, see Fig. 3(a), the portion of the lowest "ATI" peak lying below the threshold increases in strength, while the portion above the threshold decreases, as the laser intensity is increased. This is reflected by the increase of total excitation and decrease of total ionization probability shown in Fig. 1(b) in this intensity region. The trend is different from $1.70I_0$ to $1.79I_0$ [Fig. 3(b)], where the first ATI peak lies almost entirely below the threshold, with decreasing strength as the intensity is increased, while the strength of the second ATI peak, which lies above the threshold, increases with the laser intensity. This trend explains the decrease of total excitation and increase of ionization seen in Fig. 1(a) in the $1.70I_0$ to $1.79I_0$ region. Thus the out-of-phase oscillation between excitation and ionization probabilities can be understood based on the multiphoton ionization picture, as the lowest ATI peak shifts into the below-threshold region. This also explains why total excitation peak always occurs after each channel closing threshold. The numerical results of Fig. 1(b) supports this general observation. Figure 3(c) offers a different scenario where both excitation and ionization increase as the laser intensity increases. The behavior of the first ATI peak again explains how this occurs, since the first ATI peak increases in strength and this peak straddles the threshold.

While individual peaks in Fig. 3 have been discussed in terms of nonresonant ATI peaks, a closer examination shows that this is not a complete description. For the 10 fs pulses used in the calculation, the bandwidth is 0.0066 a.u., while most of the peaks seen in Fig. 3 are at least twice broader. In fact, some peaks show substructures. This is further examined in connection with the so-called Freeman resonances.

Freeman resonance occurs when an ac Stark shifted excited state $|i\rangle$ is resonantly excited by absorbing $(N - 1)$ photons,
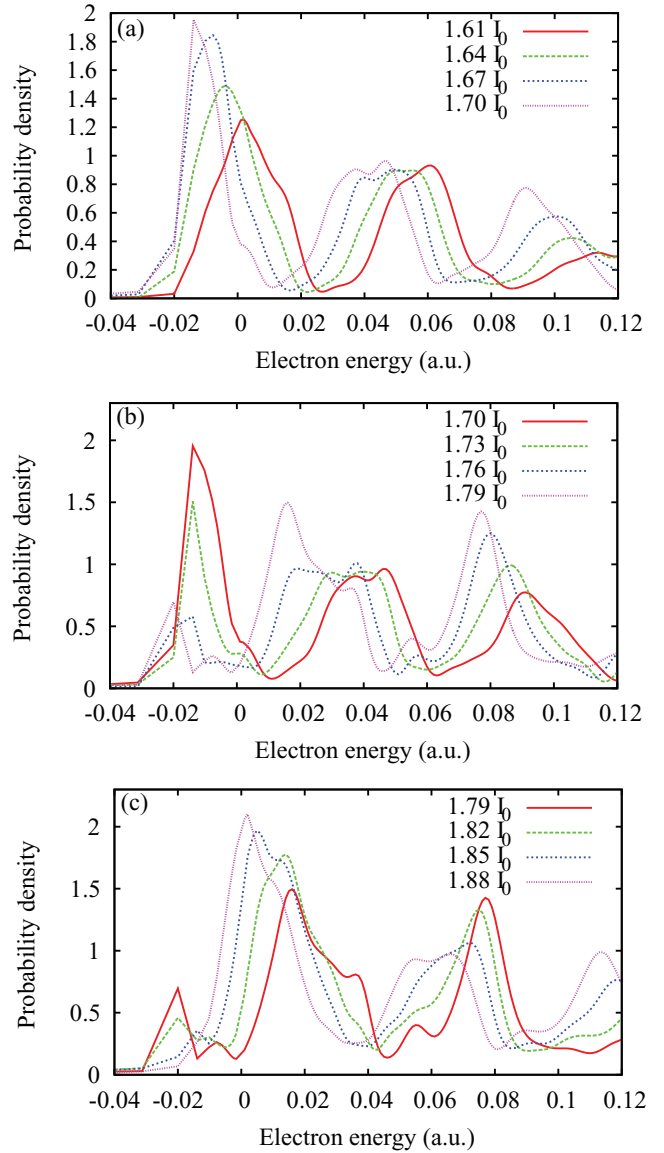

FIG. 3. (Color online) Detailed electron spectra below and above the ionization threshold for intensities between two channel closing thresholds (15 and 16 photons). Below the threshold the excited state probability is expressed in terms of probability density per unit energy (see text) as in the continuum states, thus the ATI peak is extended to the below-threshold region. Note that each ATI peak is much broader than the bandwidth of the 10 fs pulse, as the result of contributions from Freeman resonances.

i.e, $E_i + U_p = (N - 1)\hbar\omega$ at intensity I, where E_i is the excitation energy from the ground state. Such resonances are observed in the electron spectra if these excited states absorb one more photon, thus appearing near the N photon (or the first ATI) peak in the electron spectra. In Fig. 4 we show the detailed electron spectra from below to above the threshold at two laser intensities, with the positions of excited states and the expected Freeman resonances indicated. With 10 fs pulses, the bandwidth is large, thus individual Freeman resonances cannot be identified, but the bumps seen in the continuum electron spectra are consistent with such an interpretation.
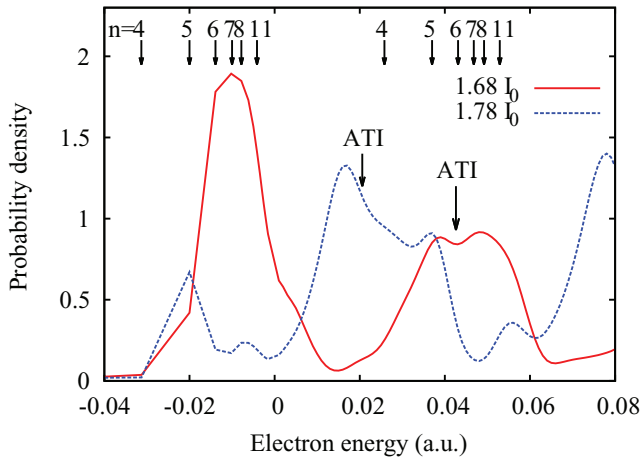
FIG. 4. (Color online) Analysis of generalized electron spectra (including bound states) at two intensities, $1.68I_0$, where excitation probability is at the local maximum, and $1.78I_0$, where excitation is at the minimum. The theoretical ATI peak positions and the expected positions of Freeman resonances are indicated. At both intensities contribution from the $n = 5$ states can be identified.

FIG. 6. (Color online) The population of excited states for different laser intensities for 10 fs pulses. The peak position in the n distribution shifts with laser intensity, in relation to the shift of the first ATI peak with the laser intensity.

C. Distributions of excited states

Figure 1(a) shows that total excitation probability within 1.0–$2.5I_0$ is at most a few percent. The total probability remains nearly constant above $1.6I_0$, in contrast to total ionization which continues to grow rapidly with intensity. Since it takes from 13 to 18 photons to ionize the hydrogen atom in the 1.0–$2.5I_0$ range, it would take 12–17 photons to reach the excited states. Since absorption of one photon increases or decreases the angular momentum by one unit, we can estimate that the dominant l should be around 5 or 6 for the populated excited states, with the distribution skewed toward higher l because the branching ratio for increasing one unit of angular momentum is higher than decreasing one in photoabsorption.

Figure 5(b) shows the normalized distributions of $l = 5$ and $l = 6$ for the excited states over the 1.0–$2.5I_0$ region, with other l's contributing a total of less than 50% at most intensities.

Figure 5(a) shows the $n = 5$, 6, and higher n distributions, again normalized for each intensity to the total excitation probability. Note that $n > 6$ distributions can account for up to 80% of the excited states at some intensities. The intensities where they peak coincide closely with the peaks of the total excitation probabilities in Fig. 1(a). In other words, these high-n states are populated most efficiently slightly after each channel closing threshold, as the lowest ATI peak dives below the ionization threshold. These high-n states have $l = 5$ or 6 mostly.

Figure 6 shows the distribution of excited states from $n = 5$–16 at four intensities from 1.50 to $1.68I_0$. From Fig. 1(a) the total excitation probability in this intensity range goes from minimum to maximum. The high $n > 6$ probabilities do not drop rapidly, especially in the intensity region where the total excitation is near the peak. Similar behavior of the n distribution has been observed at higher intensities. They show
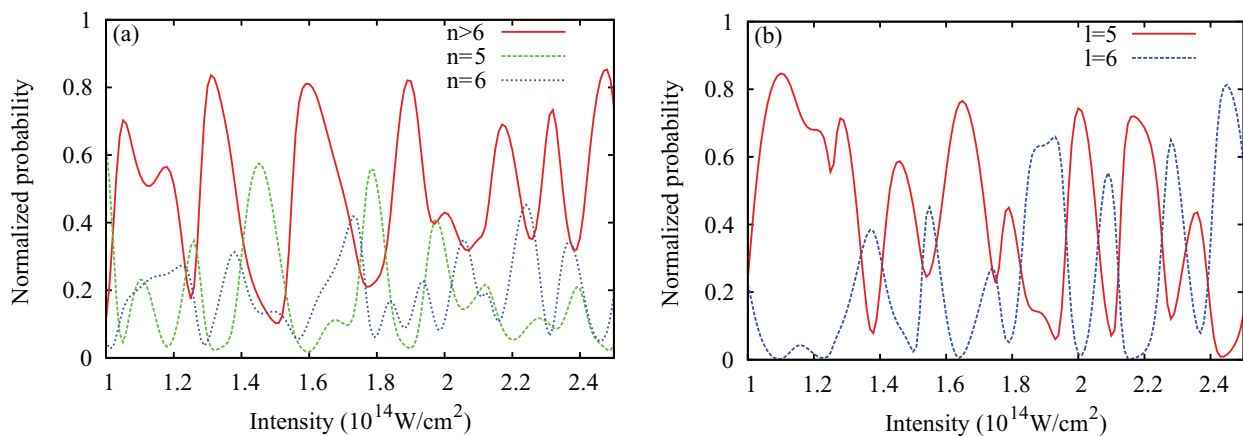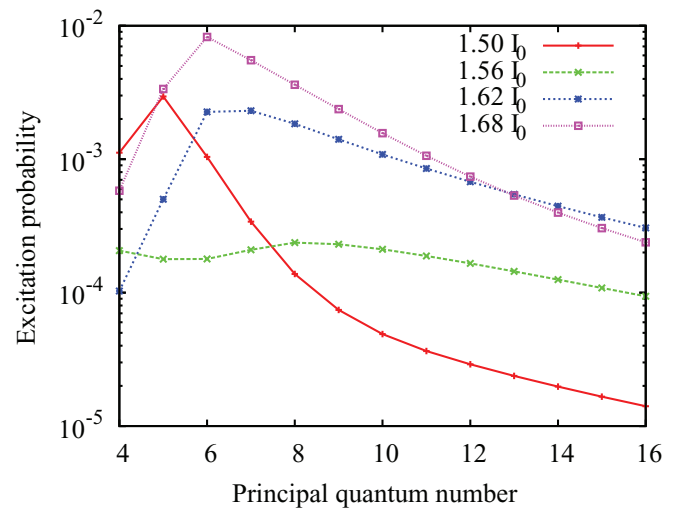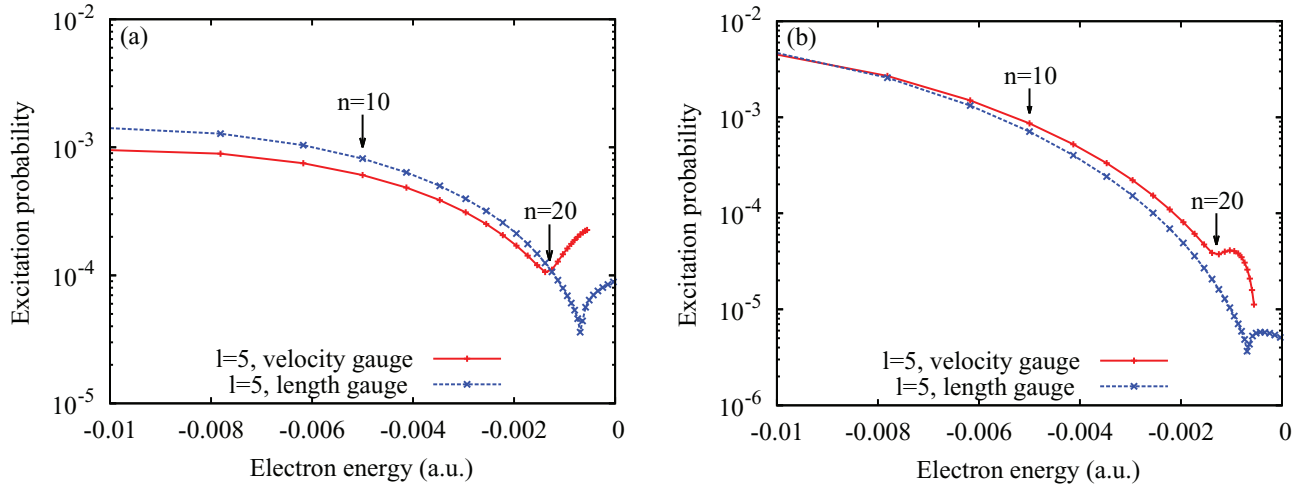

FIG. 5. (Color online) The dominant n (a) and l (b) distributions of excited states. The n distributions are normalized for each intensity to the total excitation probability, and the l distributions are normalized for each intensity to the total population with $n > 6$. These high-n states have $l = 5$ or 6 mostly, and are not easily further ionized by absorbing one photon from the laser field.

FIG. 7. (Color online) n distribution for a given dominant l, at (a) $1.61I_0$ and (b) $1.68I_0$, corresponding to minimum and maximum excitation probabilities, respectively, calculated using both the velocity and length gauges. Discrepancies between the two methods begin to appear when the probability is smaller than 0.001. Results become inaccurate for high n due to the limit from the size of the "box" used or from numerical accuracy when the probability drops below 10^{-4}.

indeed that high-n Rydberg states survive the intense 800-nm laser fields.

Figure 7 gives the probability distributions for excitation to different n states for a given l indicated at two laser intensities, $1.61I_0$ and $1.68I_0$, with results from the velocity and the length gauges. Since the radial size of the velocity gauge is smaller, the probabilities for $n > 19$ become inaccurate. For the length gauge calculation, results for $n > 27$ become inaccurate. The figures show that discrepancies between the two calculations become discernible for probabilities less than 0.001. These results indicate the high-n states are those with angular momentum quantum number close to $l = 5$. Since linearly polarized laser light is used, this means the states all have $m = 0$.

The results just presented show that high-n excited states are populated for atoms in an intense laser field. Depending on the minimum number of photons N needed to ionize an atom, we can estimate that the main orbital angular momentum would be about $l_0 = N/2$. In the tunneling ionization regime, l_0 will be near 5, 6, or higher, thus these high Rydberg states all have large l. The high-l states have little probability near the nucleus or ion core, thus an electron in such a state cannot absorb an additional photon from the laser field and it will not be ionized. This is the "mechanism" of population trapping for Rydberg states for atoms or molecules in an intense laser field. This mechanism can be extended even to the overbarrier ionization regime [18].

To support this qualitative interpretation in terms of actual numbers, we have calculated the ionization probability of high-l, high-n Rydberg states by 800-nm pulses using the first-order perturbation theory. The probabilities given in Fig. 8 are calculated for a flat-envelope pulse with duration of 5 fs at a constant intensity of 10^{14}W/cm^2. These first-order probabilities scale linearly with pulse duration and intensity, and thus can be used to estimate the ionization probability for a given pulse. For the pulse duration and intensity used in typical laser-atom experiments, the ionization probability for $n > 6$ can be estimated from Fig. 8. If the probability is less than a few percent, the excited state is considered stable

against absorption of another photon. From Fig. 8, one can expect that depletion of $l \leqslant 4$ Rydberg states by the laser field could become significant, but not for Rydberg states that have $l = 5$ and 6 or higher. Thus high Rydberg states can be formed in the early part of an intense laser pulse. The high-l Rydberg states formed will not be ionized by absorption of another photon. This discussion is not based on a specific target atom or molecule, thus it is a general
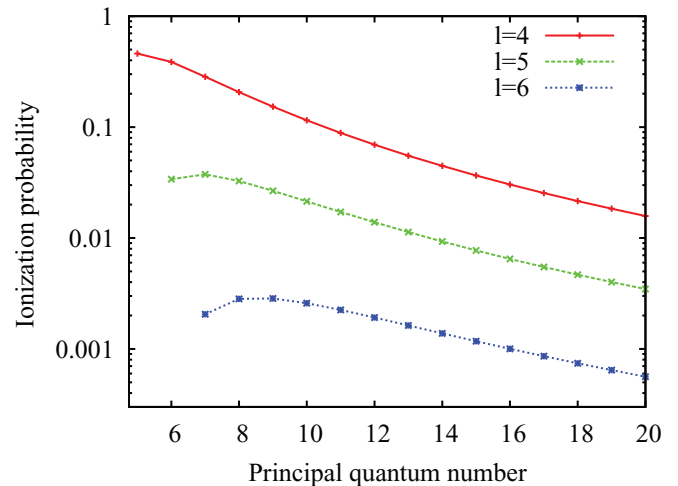

FIG. 8. (Color online) Single photon ionization probability of high Rydberg states with $l = 4$, 5, 6 by 800-nm lasers. The calculation was carried out using first-order perturbation theory for a monochromatic light with intensity of 10^{14} W/cm^2. The probabilities are shown for a duration of 5 fs. The probability scales linearly with laser intensity and with pulse duration. This figure can be used to estimate the probability of ionization of Rydberg states in an intense 800-nm laser pulse. If the resulting probability is close to 0.1 or more, then the number obtained from the figure is incorrect because the data were obtained from first-order perturbation theory. If the calculated ionization probability is less than 0.1, the Rydberg state can be considered stable against ionization by the laser field such that "population trapping" occurs for such a state.
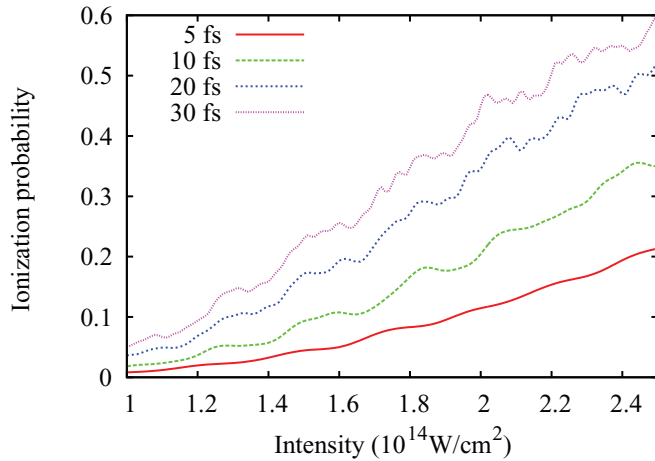
FIG. 9. (Color online) Total ionization probabilities for pulse durations of 5, 10, 20, and 30 fs, respectively, vs the intensity of the laser. The probability does not scale linearly with pulse duration due to saturation at higher intensity or to population trapping of the excited states.

phenomenon for atoms and molecules in an intense laser field. The observed "population trapping" of Rydberg states is due to the fact that high-l Rydberg states do not absorb 800-nm photons. Thus our interpretation of the presence of high Rydberg states in intense laser fields does not require the second-order Raman processes for "interference stability," nor the rescattering followed by photorecombination processes in the "frustrated tunnel ionization" model [17] that would incur emission of additional photons.

Finally, we note that total excitation probability for the 10 fs pulse does not increase for intensities higher than $1.6I_0$, see Fig. 1(a). At lower intensity, the excited states are continuously generated during the pulse. As the field intensity increases, the low-n and low-l excited states will be depleted by the absorption of one more photon. When the production and destruction of the excited states balance out, the total excitation probability would not change anymore. This can be used to explain the saturation of excitation probability at higher

intensities. Oscillation of excitation probability still would occur since the production of excited states is associated with the occurrence of channel closing, as explained earlier.

Direct observation of excited states in atoms after interacting with an intense laser has been reported in a number of experiments. Their existence also have been postulated in the interpretation of the observation of neutral atoms or molecules in a few high-intensity laser measurements. These excited atoms exist in high-n states. They are better described together as a coherent wave packet in the field. This wave packet is highly polarizable and would possess a large dipole moment. Such a highly polarizable Rydberg atom can then experience a very large force in a spatially nonuniform laser field, as reported in an earlier experiment [26].

D. Pulse duration dependence

The results presented so far are limited to 10 fs pulses and intensity below $2.5I_0$. They were calculated by solving TDSE using two different methods, and in each calculation convergence has been checked. As the intensity is increased, such a convergence test becomes more difficult as the parameters in the numerical calculations have to be increased substantially. This is also true when the pulse duration is increased at a fixed intensity.

Figure 9 shows the total ionization probability for intensity within $1.0–2.5I_0$, for pulse durations of 5, 10, 20, and 30 fs, obtained using the velocity gauge. At selective intensities, results from the length gauge calculations were carried out. For the 5 fs pulses, the total ionization rises nearly monotonically with intensity because of the large bandwidth of the pulse. For the 10 fs pulses, the small modulations have been analyzed earlier. For the 20 fs pulses, the modulations become larger and complicated. At intensities below $2.0I_0$, the convergence has been checked, but not at higher intensities. Similarly, for the 30 fs pulses, convergence is expected for lower intensities but could be a problem at higher intensities. The larger and more numerous modulations for the longer pulse and higher intensities may be real since Freeman resonances in general will be sharper, but they could also be due to inaccuracy in the
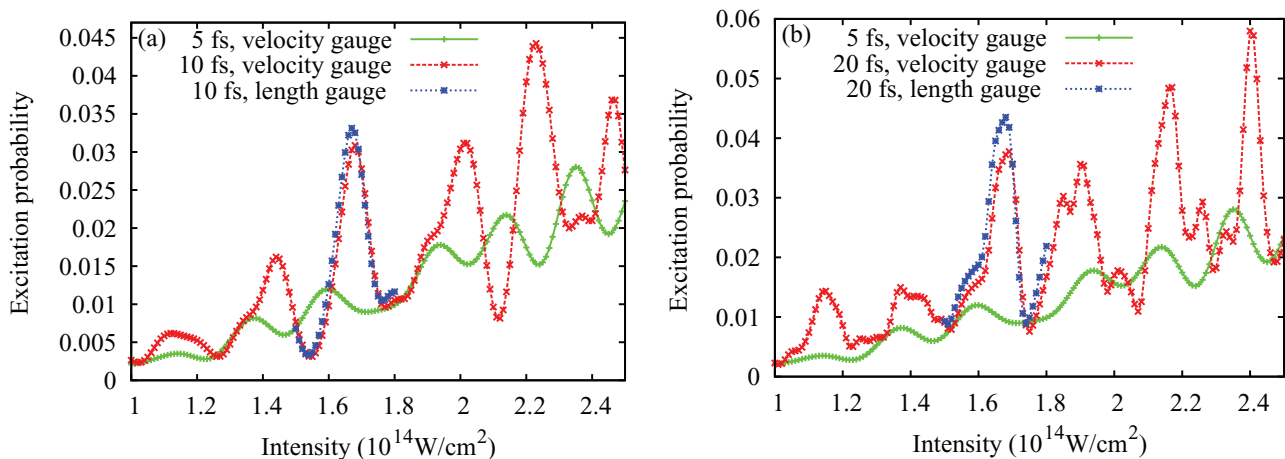

FIG. 10. (Color online) Total excitation probabilities vs laser intensities for 10 fs (a) and 20 fs (b) pulses. Results from 5 fs pulses are also shown in each panel for comparison. Main calculations are carried out using a velocity gauge. The blue symbols are obtained from length gauge—they are in good agreement with the results from the velocity gauge.
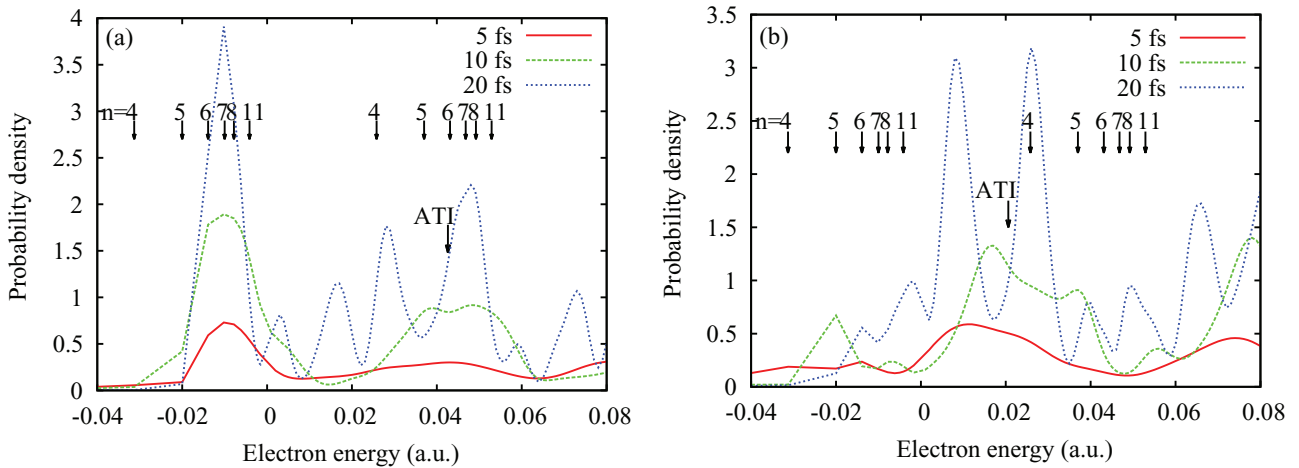
FIG. 11. (Color online) Comparison of excitation (normalized per unit energy) and ionization probability densities for 5, 10, and 20 fs pulses at two intensities, $1.68I_0$ (a) and $1.78I_0$ (b), where the total excitation probabilities are at the maximum and minimum, respectively. For 5 and 10 fs pulses, ATI peaks can be identified readily, but the much broader width of each peak indicates presence of contributions from Freeman resonances. The positions of the ATI peaks, the bound states, and the expected Freeman resonances are indicated. Some of the peaks for the 20 fs pulses cannot be easily identified with either ATI peaks or Freeman resonances. They are likely the consequence of interference between the resonant (via excited states) and nonresonant multiphoton ionization amplitudes.

numerical calculation. The main point is that highly accurate calculations for ionization of atomic hydrogen by a linearly polarized 800-nm laser pulse is not as trivial as one might like since check of convergence is not trivial without a careful investigation.

Figures 10(a) and 10(b) demonstrate the accuracy of total excitation probability calculated for 10 and 20 fs laser pulses over the 1.0–$2.5I_0$ region, respectively, obtained using the velocity gauge. These results are compared to the total excitation probabilities for the 5 fs pulses in each figure. Note that the peaks and valleys for different durations do not match very well. It is clear that the probabilities at the same intensity do not scale with the pulse duration. Within the 1.5–$1.79I_0$ range, results from the length gauge are also obtained and compared to the velocity gauge, showing good agreement between the two calculations.

Finally, in Fig. 11 we compare the excitation and ATI spectra for 5, 10, and 20 fs pulses, at two peak intensities of $1.68I_0$ and $1.78I_0$, where the total excitation probabilities are at maximum and minimum, respectively. The positions of the excited states and the expected Freeman resonances are marked by arrows. The expected first ATI peak (above the threshold) is indicated in each figure. For the 5 and 10 fs pulses, the peaks are distinct but rather broad, almost two times broader than one expected from the pulse width alone. For the 20 fs pulse, the identification of all the peaks becomes difficult. While there are peaks that can be associated with ATI peaks or Freeman resonances, there are others that cannot be assigned. The latter likely are due to interference between the broadband resonant (like Freeman resonances) and nonresonant (like ATI peaks) multiphoton ionization amplitudes.

IV. SUMMARY

In this article we analyzed excitation and ionization probabilities of atomic hydrogen in an intense 800-nm laser

field, with pulse duration up to 20 fs. The probabilities are carried out by solving the time-dependent Schrödinger equation using two independent codes with identical laser parameters. By expressing excitation probability in terms of probability density, excitation and ionization processes can be treated on equal footing. As the laser intensity is increased the ATI peak moves toward lower energies. At the intensity of channel closing the first ATI peak is centered at the ionization threshold. Upon further increase of intensity, the ATI peak moves below the ionization threshold, meaning that they would peak in the region of excited states. Thus excitation probability will peak after each channel crossing threshold. The increase of excitation is accompanied by the decrease of total ionization probability. This explains the small steps in the ion yield against a monotonically increasing background. This interpretation is not specific to atomic hydrogen. It is a general behavior of strong field ionization of atoms and molecules by intense laser fields, especially in the multiphoton ionization regime.

We further examined the stability of excited states populated in the laser field. These states tend to have large angular momentum quantum number l—they are incapable of absorbing another photon to become ionized by the laser field. This is the main reason behind population trapping of excited states. There is no need to introduce "new" mechanisms to explain the stability of high excited states of atoms or molecules in the intense laser field.

ACKNOWLEDGMENTS

[1] F. Fabre, G. Petite, P. Agostini, and M. Clement, J. Phys. B **15**, 1353 (1982).

[2] R. R. Freeman, P. H. Bucksbaum, H. Milchberg, S. Darack, D. Schumacher, and M. E. Geusic, Phys. Rev. Lett. **59**, 1092 (1987).

[3] T. Morishita, Z. Chen, S. Watanabe, and C. D. Lin, Phys. Rev. A **75**, 023407 (2007).

[4] C. M. Maharjan, A. S. Alnaser, I. Litvinyuk, P. Ranitovic, and C. L. Cocke, J. Phys. B **39**, 1955 (2006).

[5] T. Marchenko, H. G. Muller, K. J. Schafer, and M. J. J. Vrakking, J. Phys. B **43**, 185001 (2010).

[6] Y. Huismans *et al.*, Science **331**, 61 (2010).

[7] D. D. Hickstein, P. Ranitovic, S. Witte, X. M. Tong, Y. Huismans, P. Arpin, X. Zhou, K. E. Keister, C. W. Hogle, B. Zhang, C. Ding, P. Johnsson, N. Toshima, M. J. J. Vrakking, M. M. Murnane, and H. C. Kapteyn, Phys. Rev. Lett. **109**, 073004 (2012).

[8] Ph. A. Korneev, S. V. Popruzhenko, S. P. Goreslavski, T.-M. Yan, D. Bauer, W. Becker, M. Kübel, M. F. Kling, C. Rödel, M. Wünsche, and G. G. Paulus, Phys. Rev. Lett. **108**, 223601 (2012).

[9] C. I. Blaga, F. Catoire, P. Colosimo, G. G. Paulus, H. G. Muller, P. Agostini, and L. F. DiMauro, Nat. Phys. **5**, 335 (2009).

[10] W. Quan, Z. Lin, M. Wu, H. Kang, H. Liu, X. Liu, J. Chen, J. Liu, X. T. He, S. G. Chen, H. Xiong, L. Guo, H. Xu, Y. Fu, Y. Cheng, and Z. Z. Xu, Phys. Rev. Lett. **103**, 093001 (2009).

[11] J. Dura, N. Camus, A. Thai, A. Britz, M. Hemmer, M. Baudisch, A. Senftleben, C. D. Schröter, J. Ullrich, R. Moshammer, and J. Biegert, Sci. Rep. **3**, 2657 (2013).

[12] A. Talebpour, C. Y. Chien, and S. L. Chin, J. Phys. B **29**, 5725 (1996).

[13] A. Talebpour, Y. Liang, and S. L. Chin, J. Phys. B **29**, 3435 (1996).

[14] M. Fedorov and A. Movsesian, J. Phys. B **21**, L155 (1988).

[15] R. R. Jones, D. W. Schumacher, and P. H. Bucksbaum, Phys. Rev. A **47**, R49 (1993).

[16] M. P. deBoer, and H. G. Muller, Phys. Rev. Lett. **68**, 2747 (1992).

[17] T. Nubbemeyer, K. Gorling, A. Saenz, U. Eichmann, and W. Sandner, Phys. Rev. Lett. **101**, 233001 (2008).

[18] T. Morishita and C. D. Lin, Phys. Rev. A **87**, 063405 (2013).

[19] X. M. Tong, K. Hino, and N. Toshima, Phys. Rev. A **74**, 031405(R) (2006).

[20] X. M. Tong and S. I. Chu, Chem. Phys. **217**, 119 (1997).

[21] X. M. Tong, P. Ranitovic, D. D. Hickstein, M. M. Murnane, H. C. Kapteyn, and N. Toshima, Phys. Rev. A **88**, 013410 (2013).

[22] Z. Chen, T. Morishita, A. T. Le, M. Wickenhauser, X. M. Tong, and C. D. Lin, Phys. Rev. A **74**, 053405 (2006).

[23] M. V. Ammosov, N. B. Delone, and V. P. Krainov, Zh. Eksp. Teor. Fiz. **91**, 2008 (1986) [Sov. Phys. JETP **64**, 1191 (1986)].

[24] A. M. Popov, O. V. Tikhonova, and E. A. Volkova, J. Mod. Opt. **58**, 1195 (2011).

[25] A. Azarm, S. M. Sharifi, A. Sridharan, S. Hosseini, Q. Q. Wang, A. M. Popov, O. V. Tikhonova, E. A. Volkova, and S. L. Chin, J. Phys: Conf. Ser. **414**, 012015 (2013).

[26] U. Eichmann, T. Nubbemeyer, H. Rottke, and W. Sandner, Nature (London) **461**, 1261 (2009).